Design Criteria, Operating Conditions, and Nickel–Iron Hydroxide Catalyst Materials for Selective Seawater Electrolysis

Fabio Dionigi, Tobias Reier, Zarina Pawolek, Manuel Gliech, and Peter Strasser*[a]

Seawater is an abundant water resource on our planet and its direct electrolysis has the advantage that it would not compete with activities demanding fresh water. Oxygen selectivity is challenging when performing seawater electrolysis owing to competing chloride oxidation reactions. In this work we propose a design criterion based on thermodynamic and kinetic considerations that identifies alkaline conditions as preferable to obtain high selectivity for the oxygen evolution reaction. The criterion states that catalysts sustaining the desired operating current with an overpotential < 480 mV in alkaline pH possess the best chance to achieve 100 % oxygen/hydrogen selectivity. NiFe layered double hydroxide is shown to satisfy this criterion at pH 13 in seawater-mimicking electrolyte. The cata-

lyst was synthesized by a solvothermal method and the activity, surface redox chemistry, and stability were tested electrochemically in alkaline and near-neutral conditions (borate buffer at pH 9.2) and under both fresh seawater conditions. The Tafel slope at low current densities is not influenced by pH or presence of chloride. On the other hand, the addition of chloride ions has an influence in the temporal evolution of the nickel reduction peak and on both the activity and stability at high current densities at pH 9.2. Faradaic efficiency close to 100 % under the operating conditions predicted by our design criteria was proven using in situ electrochemical mass spectrometry.

1. Introduction

Water splitting by electrolyzers or photoelectrochemical devices provides a sustainable route to efficiently convert and store energy that comes from intermittent renewable resources. The electrolysis of water produces hydrogen and oxygen gas ($2\,H_2O \rightarrow 2\,H_2 + O_2$) that can recombine in a fuel cell releasing most of the stored energy and clean water as the only by-product.

Many electrocatalytic systems were investigated over the past decades, mainly operating with electrolytes consisting of high purity distilled water to which acids, bases, or buffer systems were added.[1] Only a few studies report investigations concerning the use of seawater in electrochemical[2] and photoelectrochemical[3] water splitting devices. The direct use of seawater instead of fresh water or distilled water offers tremendous advantages for implementation of electrolyzers and solar driven photoelectrochemical devices in areas where fresh water is scarcely available or the use of fresh water by the electrolyzer will constitute a competing drain of water from the local fresh water reserve. Seawater is available in sufficient quantities on the planet (~97 % of the total water) and has a fairly homogeneous geographic distribution, clearly reducing

competition with the use of fresh water by other human activities. Furthermore, arid zones will benefit from the combination of a seawater electrolyzer with a fuel cell, as this technology will not only provide a way to store energy in chemical fuel, but will also produce fresh drinking water from seawater.

Electrochemical water splitting is an energetically uphill process involving the hydrogen evolution reaction (HER) at the cathode and the oxygen evolution reaction (OER) at the anode. High activity and faradaic selectivity is particularly demanding for OER:
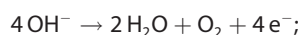
$$4\,OH^- \rightarrow 2\,H_2O + O_2 + 4\,e^-;$$
$$E^0 = +1.23\,V_{SHE}\ \text{or}\ E^0 = +1.23\,V - 0.059\,pH$$

because of its extremely poor kinetics originating from the fact that OER is a multi-electron reaction (four electrons per oxygen molecule), requiring the removal of four protons and involving more than one intermediate.[4] As a result, an energy barrier is associated with the formation of every intermediate. The design of a single catalyst that minimizes all of these barriers is not an easy task.

Dealing with seawater in water splitting devices is challenging owing to the variety of dissolved ions that can affect the catalytic system. Their average molar concentration is ~0.599 M, corresponding to an average global salinity of ~3.5 %. Dissolved ions in the electrolyte may poison or accelerate degradation of the water splitting catalysts through the formation of soluble complexes at both cathode and anode. Even more compromising to the operation of a seawater elec-

[a] Dr. F. Dionigi, Dr. T. Reier, Z. Pawolek, M. Gliech, Prof.Dr. P. Strasser
The Electrochemical Energy, Catalysis, and Materials Science Laboratory
Department of Chemistry, Chemical Engineering Division
Technical University Berlin
10623 Berlin (Germany)
E-mail: pstrasser@tu-berlin.de
Supporting Information for this article can be found under http://dx.doi.org/10.1002/cssc.201501581.

trolyzer is the fact that anions, such as, chloride, give rise to undesired competing electrochemical reactions at the electrolyzer anode, liberating undesired side products, such as, for instance, molecular chlorine or chlorinated oxidants.

However, despite the chlorine evolution reaction (ClER) competition with OER in seawater electrolysis, it is worthy to mention that both anodic electrode processes have no doubt a high importance in technologies aimed at chemical energy conversion or industrial synthesis of chemicals.[5] Indeed, chlorine is a valuable intermediate product in industry and is produced at large scale by electrolysis of brine. In the case of ClER, OER is now the undesired reaction owing to its role in accelerating degradation of the catalyst layer. Therefore, the search for more selective and stable materials, as well as deeper fundamental understanding of the mechanism behind improvements in selectivity, are of great interest.[6] According to data provided by the World Chlorine Council (WCC)[7] and the Center for European Policy Studies (CEPS),[8] the world chlorine demand is attested at ~60 million metric tonnes per year (2012), confirming the importance of this reaction. However, we believe that OER is favorable with respect to ClER when seawater is employed in processes aimed to store energy from intermittent renewable sources for the following reasons. The first problem arises from the fact that chlorine is a difficult product to handle and transport. For this reason, in industry, chlorine is essentially always generated on site and on time at the production factory where it is utilized as raw material. Indeed the high transportation costs limit the amount of chlorine transported to 5–6 % in Europe (Eurochlor 2012 annual review).[9] The generation of H_2 by intermittent renewable energy will then have to match the local chlorine demand and the electrolyzer must be located at a factory where chlorine is directly utilized, limiting the applicability in specific areas. Furthermore, the projected H_2 demand in a future global scale hydrogen economy will greatly overcome the chlorine demand by orders of magnitude, ultimately making oxygen the best co-product in hydrogen generation processes for renewable energy storage application.

Selective hydrogen production by water splitting without liberating unmanageable amounts of poisonous chlorine gas, therefore, requires extremely selective OER catalysts or precisely tuned operating conditions for selective OER. Little work was done in this area and this gap in our knowledge of the scientific basis of selective seawater electrolysis is what the present contribution addresses.

Among the catalysts proposed for OER in alkaline environments, where economically attractive non-noble metal-based materials can be used, NiFe mixed oxides and hydroxides were shown to possess relatively low overpotential and high stability.[10] Recently these materials were also successfully employed on photoanodes as protection layers and surface modifications.[11] For seawater applications these materials are unexplored to date. Therefore, we focused our study on these materials.

In this work, we propose and utilize a general design criterion for oxygen-selective seawater oxidation electrocatalysis. The criterion specifies the maximum allowed OER overpotential as a function of pH that ensures selective seawater splitting under suppression of any chlorine redox electrochemistry. Following our selectivity criterion, we show that the activity, stability, and selectivity of NiFe layered double hydroxide (LDH) are not compromised by the presence of chloride ions, while operating inside the design criterion. In contrast, under electrolysis conditions outside the selectivity criterion, we experimentally verify the predicted competition of chlorine redox chemistry associated with severe catalyst degradation. Taken together, our study demonstrates the scientific feasibility of selective operating conditions for seawater electrolysis using NiFe LDH catalysts; then shows possible technologically-viable direct seawater electrolysis.

2. Experimental

2.1. Synthesis of NiFe layered double hydroxide

NiFe LDH was synthesized by solvothermal method. First, 79.6 mg of nickel(II) acetate tetrahydrate [$Ni(C_2H_3O_2)_2 \cdot 4H_2O$] and 25.8 mg of iron(III) nitrate nonahydrate [$Fe(NO_3)_3 \cdot 9H_2O$] were hydrolyzed in ~2.4 and 1.6 mL of Millipore water. The starting molar ratio of Ni/Fe is 5. Then the two solutions were added to a mixed solution of 30 mL of water and 16 mL of anhydrous N,N-dimethylformamide (DMF) directly in the glass liner of a stainless steel autoclave (Roth, 100 mL/100 bar Model I). After 5 min of ultrasonication, the solvothermal reaction was performed at 130 °C for 16 h followed by a second solvothermal treatment at 170 °C for 2 h. Magnetic stirring was employed only for the first 30 min of the low temperature step. At the end of the synthesis, the autoclave was let cooled down naturally. The obtained suspension was ultrasonicated briefly and divided into two. One half was mixed with 44.2 mg of carbon Vulcan powder (Cabot XC-72R) and ultrasonicated. After aging overnight, the suspension was washed with a centrifuge for two times in ethanol/water mixture and two times with pure water (8500 rpm, 10 min). The samples were then freeze dried overnight.

2.2. Ink preparation

For electrochemical measurements a catalyst ink was prepared. 5 mg of supported catalyst was weighted in a glass vial. Then 500 μL of MilliQ water, 750 μL of isopropanol and 5 μL of Nafion solution (5 wt %) were added. The solution was ultrasonicated with a 1/8 in microtip sonifier for 30 min. 5 μL of ink were drop casted on a previously polished and cleaned glassy carbon (GC) electrode (5 mm of diameter) and dried in an oven at 60 °C for 7 min. The catalyst loading, including carbon Vulcan support, is about 0.1 mg cm^{-2}.

The GC disks were polished manually with a 1.0 and 0.05 μm micropolish alumina suspension for ~3 min each before each catalyst coating. After polishing, the disks were cleaned three times by ultrasonication in water, acetone, and water and finally dried with a nitrogen flow.

2.3. Materials characterization

TEM images were acquired by a FEI TECNAI G2 20 S-TWIN transmission electron microscope with LaB_6 cathode. The microscope operated at an accelerating voltage of 200 kV. Energy-dispersive X-ray spectroscopy (EDX) data were taken by an EDX detector. The catalyst powders were suspended in ethanol; then a carbon coated copper grid (400 mesh, Plano) was immersed in the solution and dried in an oven at 60 °C. Inductively-coupled plasma optical emission spectroscopy (ICP-OES) data were obtained by a 715-ES-ICP analysis system (Varian). The phase of the as-synthesized NiFe LDH nanoplates was examined by XRD. XRD patterns were collected using a D8 Advance-Diffractometer (Bruker) equipped with a Lynx Eye Detector and using a $Cu_{K\alpha}$ source.

2.4. Electrochemical measurements

Electrochemical experiments were performed in a three-compartment glass cell with a rotating disk electrode (RDE, 5 mm in diameter of GC, Pine Instrument) and a potentiostat (Gamry) at room temperature. A Pt-mesh and a Hydroflex reversible hydrogen electrode (RHE, Gaskatel) were used as counter electrode and reference electrode, respectively. The counter electrode was placed in a compartment that was separated by a fine-porosity glass frit from the working electrode compartment and a Luggin capillary was used for the reference electrode. A titanium shaft was used to prevent corrosion in case of chlorine evolution.

The electrolytes were prepared with KOH pellets (semiconductor grade, 99.99 % trace metals basis, Aldrich), H_3BO_3 (Emsure, ACS, ISO, Reag. Ph Eur, Merck), NaCl (99.5 + %, ACS, Chempur), and MilliQ water. The borate buffer was prepared with H_3BO_3 and KOH pellets that were added to reach the desired pH of ~9.2. All electrochemical measurements were carried out in N_2-saturated and rotation rate of 1600 rpm and repeated at least 3 times. All the current density (J) values reported are normalized by the geometric area (0.196 cm²). Internal resistance (iR) correction was applied after the measurements by using the value of resistance obtained during electrochemical impedance spectroscopy (EIS). All the potentials reported are iR-corrected, unless otherwise stated. Averaged values are reported in the supporting online information.

Cyclic voltammetry

Cyclic voltammetry (CV) was conducted at the sweep rate of 50 mV s⁻¹. The CVs were performed by cycling 50 times the (not iR-corrected) between 1 and 1.9 V versus RHE for both the two chloride free electrolytes, between 1 and 1.75 V vs RHE for the chloride containing electrolyte at pH 13 and between 1 and 1.8 V vs RHE for the borate-buffered chloride-containing electrolyte at pH 9.2. The different potential range was chosen to have similar iR-corrected potential range for the chloride-free and chloride-containing electrolyte at each pH (from 1 to ~1.75 V vs. RHE for both the borate buffer electrolytes at pH 9.2 and from 1 to ~1.65 V vs. RHE for the two electrolytes at pH 13).

Linear sweep voltammetry

After the CV, linear sweep voltammetry (LSV) measurements were conducted by sweeping the potential (not iR corrected) from 1.2 to 1.9 V versus RHE at a scan rate of 10 mV s⁻¹.

Stability test

Stability tests were conducted by performing chronopotentiometry (CP) at constant current of 1.96 mA ($J = 10$ mA cm⁻²) for 2 h. A pretreatment consisting of 5 cycles was performed before each CP test. A volume of electrolyte of ~50 mL was used in the stability tests that were aimed at detecting possibly dissolved metals in the electrolyte after the test. The measurements that were aimed at electrolyte titration were conducted in a small three-compartment glass cell containing ~40 mL total electrolyte to concentrate possibly produced oxidized chlorine species. In case of borate buffer + NaCl, the experiment was interrupted after the catalyst film breakdown.

2.5. Hypochlorite titration analysis

Iodide titration was performed immediately after the stability test. 20 mL of electrolyte were pipetted from the working electrode compartment to an Erlenmeyer flask. Then 15 mL of freshly prepared 0.5 M KI solution was added under magnetic stirring. In case a color change was observed, a 0.01 M thiosulfate solution was added dropwise using a burette. When the color of the solution became a faint yellow, 1 mL of starch solution was added, turning the solution blue. The thiosulfate addition was interrupted when the solution became transparent. The amount of mol of oxidized chloride species is calculated by first obtaining the mol of reacted thiosulfate by multiplying the volume difference in the burette by the concentration of thiosulfate solution. Then this value is divided by the volume of electrolyte pipetted for the titration and multiplied by the total volume of the electrolyte. For every stability test the procedure was averaged over two titrations. The corresponding charge is obtained by multiplying the amount of mol by the Faraday constant and by 2, assumed as the number of electrons per oxidized chloride species. Then this value is divided by the total charge passed during the stability test to obtain the percentage of charge associated with the formation of oxidized chloride species.

2.6. Selectivity measurements with quadrupole mass spectrometer

A two-compartment glass cell with the compartments separated by an anion-exchange membrane (Fumapem FAA-3-PK-130 from Fumatech) was used for the selectivity measurements with a RDE (10 mm in diameter of GC) and a potentiostat (Biologic) at room temperature. The area of the membrane was ~4.9 cm². The rotor and shaft were specifically made and as-

sembled to resist chlorine corrosion and be gas tight. A Pt-mesh and a saturated calomel electrode (SCE) were used as counter electrode and reference electrode, respectively. A Luggin capillary was used for the reference electrode and the distance between the working and the counter electrode was roughly 8 cm. The working electrode compartment has a glass outlet in the top part for gas product detection and an aperture (gas inlet) connected with a glass tube through which N_2 was bubbled in the solution. The SCE was calibrated versus RHE at pH 13 and the potentials reported in the paper were normalized with respect to RHE by adding 1.014 and 0.790 V for the potential at pH 13 and pH 9.2 respectively. The total metal loading on the working electrode was 7.92 μg cm^{-2}, obtained by drop casting 20 μL of ink prepared with a catalyst supported powder with 7.8% weight metal loading. The total catalyst loading, including carbon Vulcan support, is about 0.1 mg cm^{-2}. Therefore, the same metal loading per area and catalyst loading per area were used, as in the other electrochemical experiments, despite the larger electrode area.

A quadrupole mass spectrometer (QMS, Thermostar from PfeifferVacuum) was used to detect evolved chlorine and to determine the selectivity towards OER. A capillary connected with the QMS was inserted in a septum of the glass cell. The QMS was calibrated by a gas mixture of chlorine (52.1$\pm$5 ppm), oxygen (152$\pm$2 ppm), and N_2 from a pre-mixed bottle (Linde). The partial pressures of the gas in the pre-mixed bottle are given by the supplying company. chlorine ($m/z=$70), oxygen ($m/z=32$), N_2 ($m/z=28$), carbon dioxide ($m/z=44$) and water ($m/z=18$) were monitored with the QMS.

The electrochemical measurements were performed under constant N_2-bubbling, with a gas flow of 500 N mL min^{-1} set by a mass flow controller (MFC). CV was carried out as pretreatment (5 cycles) in all measurements. After the pretreatment, the stability was analyzed by conducting a sequence of CP measurements with constant current steps of 15 min each. The quasi-stationary conditions that were investigated allow to neglect differences in time constants for the different gases that otherwise would be important for a correct quantification of the products. For the electrolytes at pH 13, the current was incremented in the following step: 1, 3, 5, 7, 10, and 20 mA. For the electrolytes at pH 9.2 lower currents were set owing to instability: 1, 2, 3, 4, and 5 mA. All reported potentials are iR corrected.

2.8. Faradaic efficiency calculation

For the determination of OER, the faradaic efficiency the molecular oxygen concentration (detected by QMS) was normalized by the faradaic oxygen equivalent concentration (100% faradaic efficiency).

The molecular oxygen concentration in ppm was calculated by multiplying the averaged oxygen QMS ion current after background subtraction and N_2 normalization with the calibration factor, obtained by dividing the provided measured value of 152 ppm of oxygen and the measured oxygen QMS current measured during calibration after background subtraction and N_2 normalization. All the oxygen QMS ion currents measured

in the experiments and during calibration were normalized by the N_2 ion current (N_2 normalization), used as internal standard to take into account concentration changes owing to possible fluctuations in the flow or dilution of the gas by water vapor from the electrolyte. For example, assuming saturated vapor pressure of water (26 mbar, 22 °C) the partial pressure of N_2 will decrease by ~2.6% with respect to the dry mixture. In addition, owing to different electrolyte concentrations in the four electrolytes investigated, the water vapor pressure changes within ~3%. These changes do not affect our results because of our N_2 normalization.

For the faradaic oxygen equivalent concentration, the flow of N_2 was first calculated in mmol s^{-1} by using the set flow value (500 N mL min^{-1}) and the ideal gas law at standard conditions (1 atm, 273 K). A flow of 0.372 mmol s^{-1} was obtained. Finally, the electrochemical current expressed in mA was divided by 4F, where F is the Faraday constant and further divided by the nitrogen flow in mmol s^{-1}. The result was then expressed in ppm by multiplying by 10^6.

The error associated with the faradaic efficiency is obtained by considering the error on the oxygen ppm value provided by the gas bottle provider (1.3%), error on the MFC measurement (2%), error on the determination of the QMS current in the calibration experiment (0.1%), and standard error of the mean for the averaging of the oxygen QMS signal during the experiments.

2.9. Turnover frequency calculation of the catalysts

The turnover frequency (TOF) value is calculated from the equation:

$$TOF = \frac{J}{4Fm^*}$$

$$m^* = L\left(\frac{Ni_{wt\%}}{Ni_u} + \frac{Fe_{wt\%}}{Fe_u}\right)$$

where J is the current density at an overpotential of 0.3 V estimated from the LSV, F is the Faraday constant and m is the mol of metal per cm^2. m^* is obtained by multiplying the catalyst loading L (0.1 mg cm^{-2}) by the sum of the weight percentage of nickel (Ni$_{wt\%}$) and iron (Fe$_{wt\%}$) divided by their respective atomic mass (Ni$_u$ and Fe$_u$, respectively). The weight percentage of nickel and iron are obtained from ICP measurement. We notice that this TOF is a lower estimation, since it considers all the metal atoms on the GC as active sites.

3. Results and Discussion

3.1. A general design criterion for selective seawater splitting

Chlorochemistry in aqueous environments comprises a complex ensemble of possible reactions that depend on pH and concentration of chloride ions. Figure 1 displays a computed Pourbaix diagram of aqueous chlorochemistry for the conditions relevant to electrochemical OER at room temperature and total
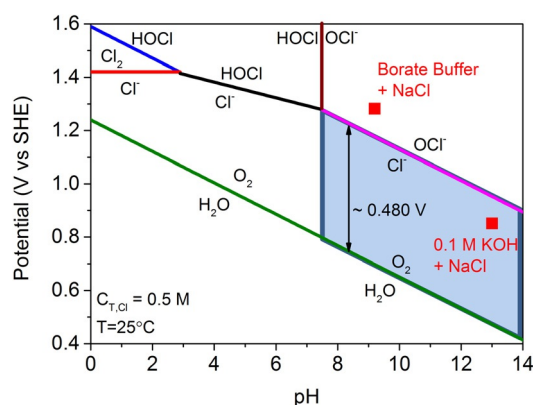
Figure 1. Pourbaix diagram for artificial seawater model. A chlorine system, in the case of dissolved 0.5 M NaCl aqueous solution and no other chlorine sources, with a total chlorine species ($c_{T,Cl}$) of 0.5 M. The electrode potential for OER is also included (assuming oxygen partial pressure of 0.21 atm = 0.021 MPa). Two red square points show the operating potentials (vs. SHE) after 1 h constant current electrolysis (10 mA cm^{-2}) with NiFe LDH catalyst in 0.1 M KOH + 0.5 M NaCl (pH 13) and 0.3 M borate buffer + 0.5 M NaCl (pH 9.2) electrolyte. The light blue box highlights our proposed design criterion.

mass of chlorine species fixed at 0.5 M. A description of the construction of the Pourbaix diagram for chlorine species is available in Ref. [12]. In acidic solutions, the ClER[13]

$$2\,Cl^- \rightarrow Cl_2 + 2\,e^- \qquad E^0 = +1.36\,V_{SHE} \qquad (1)$$

can occur and does compete with the OER. The Pourbaix diagram shows that OER is thermodynamically favored over ClER. However, ClER is a two-electron reaction that involves only a single intermediate. As a consequence, ClER has much faster kinetics than OER and is the dominant anodic reaction in acidic electrolytes on many oxide catalysts.[5, 6c, 14]

In alkaline conditions, hypochlorite formation must be considered:[13]

$$Cl^- + 2\,OH^- \rightarrow ClO^- + H_2O + 2\,e^-;$$
$$E^0 = +0.89\,V_{SHE,\,pH\,14} \text{ or } E_0 = +1.72\,V - 0.059\,pH \qquad (2)$$
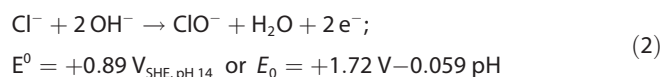
This reaction is also a two-electron reaction, so it has a kinetic advantage over OER. However, thermodynamics highly favor OER over hypochlorite formation. Furthermore, the standard electrode potential of hypochlorite formation, unlike ClER, is pH dependent and it follows the OER potential in the Pourbaix diagram (Figure 1). Therefore, the electrode potential difference to OER is fixed at ~0.480 V.

If the electrocatalyst is operating at an overpotential (η) lower than this value, hypochlorite formation cannot occur and so OER does not compete with a chlorine redox reaction with faster kinetics. A similar argument could be formulated for acid and ClER, but the difference between ClER and OER potentials in acid is smaller, making it much more challenging to reach high currents at an electrode potential where ClER is not yet thermodynamically allowed. Therefore, alkaline conditions seem preferable for seawater oxidation. Furthermore, non-noble metal-based catalysts that would degrade in acidic

can be used in alkaline conditions. Based on these considerations, we establish a general design criterion [Eq. (3)] for OER/oxygen selective operation of noble-metal-free electrocatalysts operating at pH > 7.5 in seawater electrolyte as the difference in the standard potentials (ΔE^0) between the OER and the chlororeactions, such as Equation (2):

$$\eta_{OER} \leq 480\,mV \qquad \text{at pH} > 7.5 \qquad (3)$$

The lower pH limit was taken at 7.5, the pK_a of the hypochlorous acid, below which the hypochlorous acid formation becomes dominant respect to the hypochlorite ion, and the difference of the undesired side reaction potential respect to the OER potential becomes slightly smaller. The design criterion states not the only, but the most favorable conditions to achieve high selective oxygen evolution from seawater oxidation.

The requirement to operate at $\eta_{OER} \leq 480\,mV$ and at $J = 10\,mA\,cm^{-2}$, often indicated as technological target for commercial integrated devices based on solar-driven photoelectrochemical water splitting where the photoabsorber and electrode areas are identical, or at a higher densities closer to the state-of-the-art of industrial alkaline electrolyzers, is demanding for noble-metal-free materials.

3.2. Synthesis and Structure NiFe-layered double hydroxide catalysts

NiFe LDH catalysts are known to reach such low overpotentials for OER in chloride-free alkaline electrolyte.[10c] A solvothermal method involving a mixture of water and DMF was used to synthesize NiFe LDH.[10c] The detailed protocol for the synthesis of the catalysts is presented in the Supporting Information. The synthesized NiFe LDH catalyst presents hexagonal nanoplate morphology, typical of well crystallized LDH materials (Figure 2 a–b).[15] The NiFe LDH nanoplates are decorated with smaller amorphous FeO$_x$ particles. It is known that iron that is not incorporated in the NiFe LDH can form FeO$_x$ or FeOOH nanoparticles or domains, both when the NiFe LDH is synthesized by a solvothermal/hydrothermal synthesis as well as by electrodeposition method.[10c, 16] All XRD reflections are assigned to a hydrotalcite structure, typical of NiFe LDH (Figure 2 c).[15] The solvothermal synthesized NiFe LDH presents long crystalline order, with narrow and well defined reflections. The main diffraction peak at the 2θ angle of 11.3°, labeled with the Miller indexes (0 0 3), corresponds to diffraction from planes along the stacking direction. Therefore, the d-spacing, 7.8 Å in this case, is a measure of the distance between the LDH layers. This value is compatible with NiFe LDH with intercalated carbonate anions.[17] The crystallite size obtained from the (0 0 3) peak width could be used as a gross estimate of the nanoplates thickness, under the exclusion of vertically stacked multicrystalline domains.[10c] In our case, the Scherrer equation estimates a crystalline size of 15 ± 1 nm [full-width-at-half maximum (FWHM) = 0.58°]. The difference with the 5 nm reported by Gong et al. could be attributed to the slightly higher temperature used in this work.[10c] A 3D atomic model of the ex-
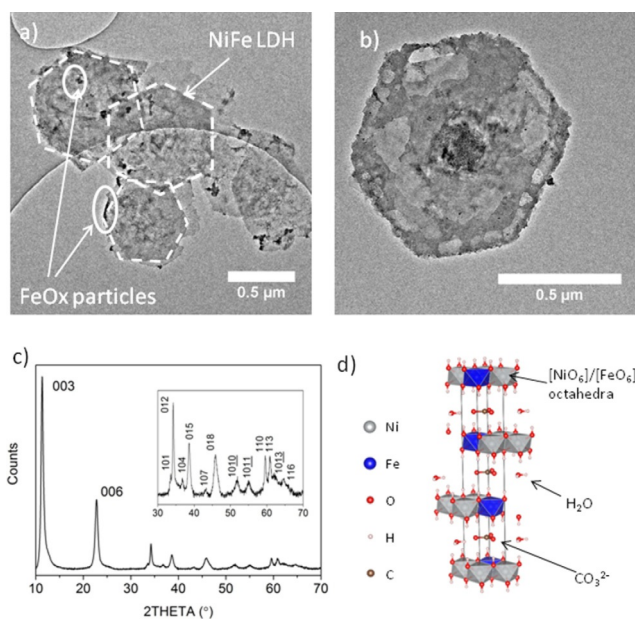
Figure 2. a) TEM image of hexagonal NiFe LDH nanoplates and smaller FeO_x particles. b) TEM image of a single hexagonal NiFe LDH nanoplate. c) XRD pattern of NiFe LDH with insert showing the higher 2θ angle range. d) 3D structure model of the as prepared NiFe LDH with intercalated water and carbonate ions.

tended unit cell of NiFe LDH in the fully protonated form and with formula $[Ni^{2+}_{1-x}Fe^{3+}_x(OH)_2]^{x+}(CO_3^{2-})_{x/2} \cdot y(H_2O)$ is presented in Figure 2d. Layer of edge sharing $[NiO_6]/[FeO_6]$ octahedra stacks along the c-axis with OH groups on both sides and water and charge balancing anions (i.e., carbonate anions) intercalated between the layers. ICP-OES and EDX were used to analyze the composition of the catalyst. ICP showed an average sample composition of 73 at % nickel and 27 at % iron, whereas the more local EDX analysis reveals that areas with few FeO_x particles have a slightly lower iron content of ~13 at %. Therefore, we consider the value of 13 at % iron a more accurate estimate of the real iron content of the NiFe LDH nanoplates.

3.3. Electrochemical seawater splitting: pH and Cl⁻ effects

The electrochemical measurements were performed using a RDE in a three-electrode system and three-compartment glass cell. An ink was prepared with NiFe LDH catalyst supported on carbon Vulcan (Cabot) and drop-casted on a GC electrode. We tested the catalysts in alkaline (0.1 M KOH, pH 13) and near-neutral electrolyte (0.3 M borate buffer corrected with KOH to reach pH 9.2, the pK_a), both in chloride free conditions and with 0.5 M of NaCl addition. In the text, the following short notations will be used for indicating the four electrolytes: 1) KOH, 2) borate buffer, 3) KOH + NaCl, and 4) borate buffer + NaCl. Borate buffer is added as a proton-accepting support in near neutral pH, to contrast changes in local pH.[2b,18] The group of Nocera, and more recently other groups, also investigated OER activity and stability of electrodeposited nickel oxide catalyst in potassium–borate solutions, showing long-

term stability under this mild pH condition.[19,20] To avoid a dramatic decrease in local pH at the anode,[21] seawater cannot be used without buffer additives. Even though carbonate and borate ions are present in seawater, their average concentration is too low to sustain proton handling at high currents. In the Supporting Information, this is shown by solving calculations based on general mass transfer equation theory for a simple model system consisting of a flat plane rotating disk electrode under stationary conditions (Figure S1 and S2 in the Supporting Information).[18,22]

Therefore, the choice of the two pH values and the supporting buffer was based on these reasons and on the previous works reported in the literature (performed in the absence of NaCl). The choice of utilizing borate buffer at pH 9.2 was also supported by a previous screening that we performed with borate (0.1 M, pH 9.2), phosphate (0.1 M, pH 7), and carbonate (0.1 M, pH 8.6 and 10) buffers, which showed that higher stability was obtained with borate buffer.[23]

Figure 3 compares the electrochemical OER performance in fresh and seawater conditions and two buffered pH conditions. After a voltammetric "break-in" treatment (50 cycles, see Figure S3), LSV was recorded at a lower scan rate to evaluate the electrochemical activity (Figure 3a). All the anodic LSVs show an anodic wave, attributed to nickel(II/III) redox reaction, characteristic of nickel hydroxide systems. The change in oxidation state of nickel is associated with a loss of proton:

$$Ni(OH)_2 + OH^- \rightarrow NiOOH + H_2O + e^- \qquad (4)$$
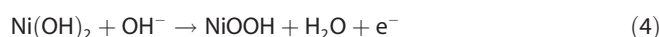
The molecular mechanism associated with the anodic wave is likely more complex than the simple deprotonation shown in Equation (4) and co-involves exchange of ions and water between the metal oxide layers.[24] At more anodic potentials an increase in J is observed and attributed to OER.

Figure 3 evidences a pronounced effect of the electrolyte pH on the electrochemical water splitting performance of the catalysts. Both the redox wave and the OER occur at more positive potentials (vs. RHE) by decreasing the pH. The OER overpotential increases ~110 mV (vs. RHE) at 1 mA cm⁻². This shift corresponds to a shift of ~87 mV per pH on SHE scale.

The shift of the oxidation peak, on the other hand, is ~85 mV per pH step in the SHE scale. Therefore both the oxidation wave and the OER show a similar super-Nernstian potential pH shift. A shift of 88 mV per pH was observed for the redox peaks assigned to the hydrous α-Ni(OH)₂ phase, in contrast to a Nernstian shift of the redox peaks in case of anhydrous β-Ni(OH)₂.[25] This is consistent with the model of the NiFe LDH as hydrous hydroxide with water intercalated between the layers. A detailed analysis of the LDH redox chemistry during break-in CVs is presented in Figure S3. Similar to what was observed in the LSV for the anodic wave, we observed a shift (in the RHE scale) towards higher potentials for both the anodic and cathodic wave in the lower pH cases. Second, the separation in potential between the redox peak maximum (for anodic) and minimum (for cathodic) increases at lower pH. This separation was evaluated for the 50th cycle in the RHE scale to be 119 ± 9 mV for pH 13 and 183 ± 10 mV for
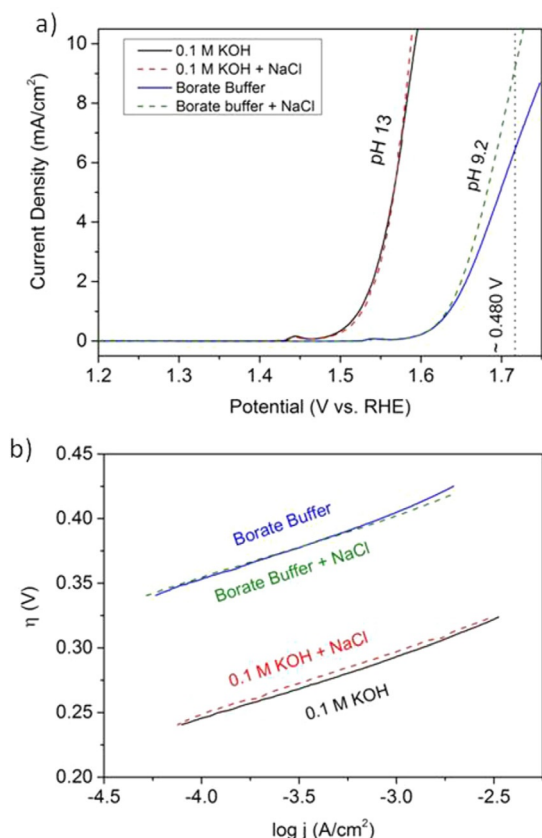
Figure 3. a) Electrocatalytic OER activities of NiFe LDH nanoplates supported on carbon, measured using LSV in four different electrolytes after CV "break-in" (50 cycles). η of approximately 480 V, corresponding to the design criteria limit, is marked by a dashed vertical line. b) Corresponding Tafel plot for low J. Measurement conditions: room temperature, 1600 rpm, scan rate: 1 mV s^{-1}. The total metal loading determined by ICP is 7.9 µg cm^{-2}. Electrolytes: (——) 0.1 M KOH, pH 13; (- - - -) 0.1 M KOH + 0.5 M NaCl, pH 13; (——) 0.3 M borate buffer, pH 9.2; and (- - - -) 0.3 M borate buffer + 0.5 M NaCl, pH 9.2.

pH 9.2. These observations seem to point to a less reversibility of the nickel redox couple at lower pH. And finally, the data show that the area of the peaks in pH 13 is larger than at pH 9.2, consistent with reduced nickel accessibility.

We now turn to the discussion of the chloride-containing seawater conditions. Our data evidence a striking effect of the added NaCl on the temporal evolution of the metal redox peaks during potential "break-in" cycling (Figure S3 a–b), that is particularly evident for pH 13. Here, the anodic peak in NaCl-free electrolyte is growing in intensity very slowly, whereas in presence of chloride and sodium ions, the metal redox peak reaches essentially the same intensity after only the 2nd cycle, as observed after the 50th cycle in NaCl-free conditions. Similarly, the cathodic peak grows slowly in chloride-free conditions, whereas, in presence of chloride and sodium ions, the redox peak starts out intense and very narrow and slowly widens at the 50th cycle. Despite different NaCl-dependent evolutions, the peaks for NaCl-containing and NaCl-free electrolyte reach similar shape and intensity at the 50th cycle, both at pH 13 and at pH 9.2 (Figure S3 b,d). This observation suggests that the presence of chloride and sodium ions accelerates the electro-

chemical access to nickel redox centers that are electrochemically active for the nickel(II/III) redox reaction and make the reduction much more easier at the beginning of the cycling process.

The overpotentials at 10 mA cm^{-2} and the Tafel slopes obtained from the LSV experiments (Figure 3 a) for the chloride-free and chloride-containing electrolytes are reported in Table 1. The experimentally derived TOF in 0.1 M KOH electrolyte at the overpotential of 300 mV amounted to ~0.03 s^{-1}. The TOF was calculated assuming all metal atoms represent active sites, that is, it represents a lower limit.

Table 1. LSV overpotential and Tafel slopes with respect to the four electrolyte conditions.[a]

Electrolyte	η[b] [mV]	Tafel slope [mV dec^{-1}]
KOH	360 ± 3	51 ± 1
KOH + NaCl	359 ± 1	50 ± 1
Borate buffer	529 ± 12	50 ± 4
Borate buffer + NaCl	490 ± 4	51 ± 3

[a] Electrolytes: 1) 0.1 M KOH, pH 13; 2) 0.1 M KOH + 0.5 M NaCl, pH 13; 3) 0.3 M borate buffer, pH 9.2; and 4) 0.3 M borate buffer + 0.5 M NaCl, pH 9.2. [b] At 10 mA cm^{-2} measured during LSV (1 mV s^{-1}).

The chloride ions do not seem to adversely affect the catalytic OER reactivity of the NiFe LDH catalysts at moderate J as can be seen from both the LSVs and the Tafel slopes in Figure 3 b. The values of the Tafel slopes at moderate current densities are similar in all cases. This may indicate a similar OER mechanism at either pH as well as in presence of chloride ions, even though attention must be paid in analyzing the Tafel slope absolute values owing to the complexity of multistep, multielectron OER.[10b] Interestingly, a similar Tafel slope in borate buffer, ~56 mV dec^{-1}, was recently obtained by Smith et al. with a NiFe electrochemically co-deposited film.[20] Notice that for both pH values, the electrode potentials during the LSVs are well inside the design criterion in the case of low J; therefore, no difference should be expected according to our model.

Surprisingly, in the case of pH 9.2, chloride ions appear to boost catalytic OER activity at higher J. Whether that boost can be entirely attributed to molecular oxygen evolution or whether by products are formed is unclear without a detailed discussion of chemical selectivity (vide infra). Generally, at the chosen pH values, chlorine should not be produced; nonetheless, this could happen if the local pH at the anode is strongly decreased by an inefficient proton abstraction and proton transport. In this case, the local acidity will negatively affect both stability and selectivity of the non-noble metal catalyst. This is why sufficient diffusive and convective mass transport at the electrolyzer electrode is crucial to maintain constant pH operation and selectivity.

3.4. Faradaic selectivity measurements using in situ mass spectrometry

To demonstrate the validity of the design criterion and rule out the formation of molecular chlorine or hypo-chloric acid within 480 mV overpotential under alkaline conditions, we carried out chemical selectivity measurements combining in situ headspace mass spectrometry with constant-current electrochemical measurements in a custom-made titanium-based gas-tight two-compartment RDE setup with an anion-exchange membrane (AEM) to minimize gas cross mixing and rotor corrosion by produced chlorine. Selectivity test measurements under acidic conditions where chlorine evolution is dominant (see Figure 1) confirmed the simultaneous detection capability of gaseous oxygen and chlorine (Figure S4). Detection limits were estimated to few ppb. To measure the faradaic efficiencies of the NiFe LDH sea water splitting catalysts under alkaline conditions, both oxygen ($m/z = 32$) and chlorine ($m/z = 70$) were monitored, while the applied J was increased in CP steps of 15 min each. The QMS ionization currents for oxygen and chlorine are reported in Figure S5.

While the oxygen signal increased stepwise with increasing current, no significant chlorine signal could be detected across the sampled current range. This means that under the current conditions the selectivity of the OER and molecular oxygen remained fairly high. At the same time, this measurement indirectly confirmed the good proton accepting efficiency of the borate buffer electrolyte preventing the local pH to drop to acidic pH where gaseous chlorine would evolve. We also estimated the faradaic efficiency for molecular oxygen by relating the ion currents (black trace, Figure S6) and faradaic currents (red steps, Figure S6) and deriving faradaic efficiencies. Figure 4 plots the faradaic efficiencies together with the applied current densities over their corresponding time-averaged electrode potentials. The corresponding detailed time traces of the electrode potentials are shown in Figure S7. The faradaic efficiency towards the OER and molecular oxygen remained close to 100 % (experimental error less than 5 %) under both pH conditions in both fresh and sea water electrolyte conditions inside the overpotential design criterion. Trace amounts of hypochlorous acid at electrode potentials outside our design criterion—mostly below detection limits—suggested that the hypo chlorite formation process [see Eq. (2)], despite being a two-electron process, is likely subject to own kinetic overpotentials, limiting the accumulation of hypochlorite ions. In all, our observations are in excellent agreement with our earlier prediction that molecular chlorine cannot form in sea water electrolysis under alkaline conditions (see Figure 1). Our selectivity measurements demonstrate the high faradaic efficiency of the NiFe LDH materials for water oxidation in seawater electrolyte while operating inside our general design criterion.
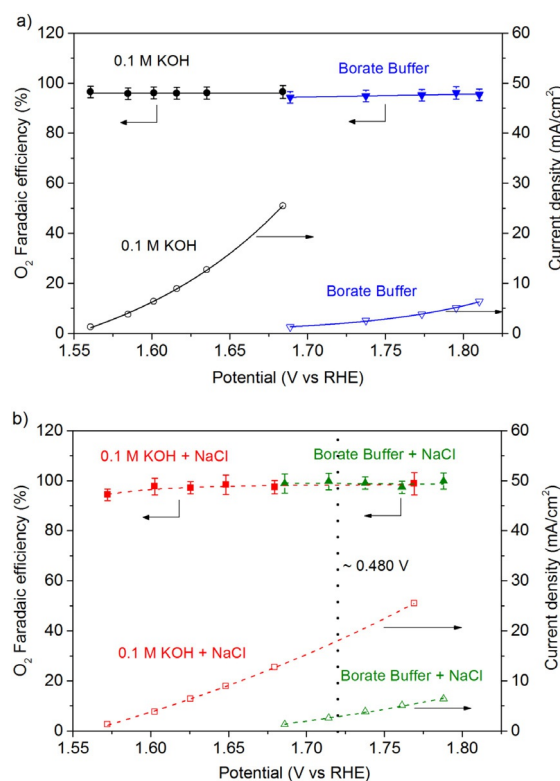

Figure 4. Faradaic efficiency of NiFe LDH on carbon support for OER (●, ▼, ■, ▲) and current density (○, ▽, □, △) as a function of averaged measured potential during constant current potentiometric steps of 15 min each. η of approximately 480 V, corresponding to the design criteria limit, is marked by a dotted vertical line. Electrolytes: (——) 0.1 M KOH, (——) borate buffer, (-----) 0.1 M KOH + NaCl, and (-----) borate buffer + NaCl. Measurement conditions: room temperature, 1600 rpm, N$_2$ bubbling. The total metal loading on the working electrode is 7.9 µg cm^{-2}.

3.5. Long-term stability and degradation in- and out-side the OER selectivity range

To address the longer-term stability of the NiFe LDH catalyst, a 2 h test at fixed J of 10 mA cm^{-2} was performed according to a recently proposed protocol.[10b] An initial activation procedure consisting of 5 CV cycles was adopted before the CP measurement. The potential recorded during the constant-current measurement is displayed in Figure 5. At pH 13, the catalyst showed a reasonably stable behavior in chloride-free conditions (black line), with an increase of the overpotential of merely ~0.04–0.06 V, similar in magnitude to values reported for electrodeposited NiFeO$_x$.[10b] In the presence of dissolved chloride ions (red line) the catalyst is able to operate well inside the critical overpotential limit of 0.480 V required for OER selectivity (horizontal dotted line). Despite the slow increase of potential, sustained selective seawater electrolysis at 10 mA cm^{-2} is feasible in the selective region. No change in the averaged nickel/iron ratio (Ni/Fe = 3.3) and no evidence for permanent incorporation of chloride anions were observed by EDX analysis after this experiment.

In contrast, the catalyst stability in the lower pH electrolyte ("Borate Buffer" in Figure 5) was generally worse. Considering the relatively high current densities associated with fast hy-
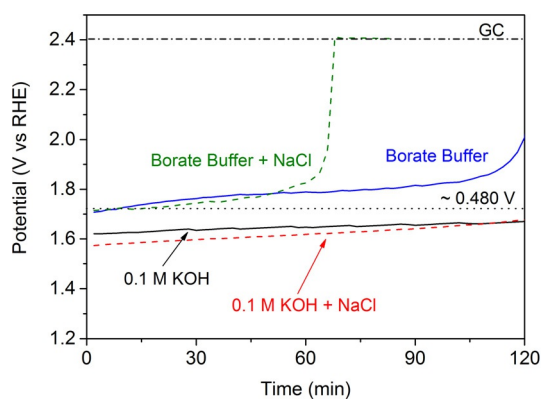
Figure 5. a) Electrocatalytic stability test of NiFe LDH on carbon support in the four electrolytes measured by 2 h CP after 5 activation cycles. The over-potential $\eta \sim 480$ V, corresponding to the design criterion limit, is marked by a dotted horizontal line. Measurement conditions: Constant $J = 10$ mA cm^{-2}, 1600 rpm. Electrolytes: (——) 0.1 M KOH, pH 13; (-----) 0.1 M KOH + 0.5 M NaCl, pH 13; (——) 0.3 M borate buffer, pH 9.2; and (-----) 0.3 M borate buffer + 0.5 M NaCl, pH 9.2. (–•–•) The potential corresponding to bare GC.

droxide removal during OER, the catalyst degradation in borate buffer could be explained by gradual support corrosion combined with catalyst dissolution owing to a reduced interfacial pH caused by a limited borate buffer capacity. In all electrolytes, catalyst degradation could be further enhanced by mechanical impact owing to the strong bubble formation.

A particularly severe corrosion of the NiFe LDH water splitting catalyst was observed in borate buffer in the presence of chloride (seawater conditions). Here, the catalyst film almost completely detached into small material flake, whereas the electrode potential sharply increased to 2.4 V after about 60 min. Figure 5 evidences that under this pH condition it is no longer possible to sustain $J = 10$ mA cm^{-2} inside the oxygen-selectivity limit. As a result of this, hypochlorite, a strong oxidant, formed hypochlorite in a two-electron process [Figure 1 and Eq. (2)]. At this bulk pH, hypochlorite ions will be present even if gaseous chlorine should locally evolve at the electrode interface owing to local acidity (low local pH owing to hydroxide removal during OER and hypochlorite formation), because molecular chlorine would immediately dissociate into hypochlorite upon diffusion into the bulk. To quantify the formation of hypochlorite we have develop and utilized a iodometric titration of the chloride-containing borate-buffered electrolyte of the working compartment. Our titration after the stability test confirmed the formation of oxidized chlorine species (HClO and OCl$^-$). In total, 2.5 µmol of hypochlorite were produced in the experiment shown in Figure 5, corresponding to ~5% of the total current passed (total charge passed ~9.878 C). Thus, the enhanced hypochlorite formation in borate buffer appears a likely cause of the reduced stability of the catalyst in borate buffer. We do note that some hypochlorite could have been produced at the bare GC support electrode after catalyst detachment. On the other hand, no hypochlorite was detected after the stability test in seawater at pH 13 in agreement with the predictions of Figure 1.

The chemical dissolution of a solid electrocatalyst by complexation with charged or neutral species is another important aspect to discuss in the context of stability. Taking the solubility product at 25 °C, $K_{sp} = 5.48$ 10^{-16} of the NiFe LDH close to that of Ni(OH)$_2$,[13] the expected free equilibrium concentration of Ni^{2+} ions in solution (Ni(OH)$_2 \leftrightarrow$ Ni^{2+} + 2 OH$^-$) is extremely low ranging from 5.48×10^{-14} M at pH 13 to 1.38×10^{-7} M at pH 9.2. Free Ni^{2+} ions form octahedral aqueous complexes, the hexa-aqua nickel(II) ions, [Ni(H$_2$O)$_6$]$^{2+}$. However, complexation of nickel ions and chloride ions to form soluble nickel chlorides could drive up the dissolution of the NiFe LDH catalyst. Indeed, under seawater conditions, some of the water ligands can be replaced by chloride ligands. It has been shown that in acidic conditions and room temperature the hexa-aqua nickel is the dominant species and the octahedral [Ni(H$_2$O)$_5$Cl]$^+$ is the only significant chloro-complex formed.[26] Other complexations, like the octahedral NiCl$_{2(aq)}$ or the tetrahedral NiCl$_3^-$ and NiCl$_4^{2-}$, become relevant only at higher temperatures (i.e., 100–200 °C and higher) or in chloride concentrations higher than 0.5 M. The logarithm of the formation constant K of [Ni(H$_2$O)$_5$Cl]$^+$ complex is log(K) = −0.42 at 25 °C ([Ni(H$_2$O)$_6$]$^{2+}$ + Cl$^- \leftrightarrow$ [Ni(H$_2$O)$_5$Cl]$^+$ + H$_2$O).[26] Therefore, the expected distribution of nickel species in 0.5 M chloride comprises [Ni(H$_2$O)$_5$Cl]$^+$ at 15% and of [Ni(H$_2$O)$_6$]$^{2+}$ at 75%. We checked for dissolution of nickel and iron in the electrolytes after the stability measurements by ICP-OES measurements and we compared the results with the fresh electrolytes. For all 8 catalyst samples no nickel ions could be detected or remained below our detection limit of 2 µg L^{-1}. Iron ions were detected in all 8 samples, with concentration fluctuating between about 2 and 7 µg L^{-1} (ppb). This result indicates that iron impurities were present in the electrolytes before testing and their amount was not significantly affected after the 2 h electrolysis. Therefore, if nickel and iron dissolution is occurring is beyond our detection limit (2 and 1 ppb corresponding to a ratio of the ICP detection limit to the highest possible metal concentration if all NiFe LDH was dissolved of 4 and 6%, respectively). We notice that, despite the 2 h test providing a valid screening for the analyzed conditions, an extended protocol is necessary to check the NiFe LDH stability in operating conditions that more closely resemble that of a commercial device (i.e., 8 h day^{-1} for a diurnal cycle or longer times for an industrial electrolyzer).

4. Conclusions

We have analyzed the competition of oxygen and chloro-electrochemistry in the context of electrochemical hydrogen production by splitting of seawater. For the first time, a rigorous general design criterion for oxygen-selective seawater splitting was derived from thermodynamic and kinetic considerations. Figure 6 summarizes our results, showing alleviated conditions for selective oxygen evolution reaction (OER) in alkaline conditions. Validity of the selectivity criterion was demonstrated using a family of noble-metal-free NiFe layered double hydroxide (LDH) electrocatalysts operated in seawater. We conclude that, at pH 13, NiFe LDH nanoplates can safely operate as OER-selective electrocatalysts in seawater inside the selective over-
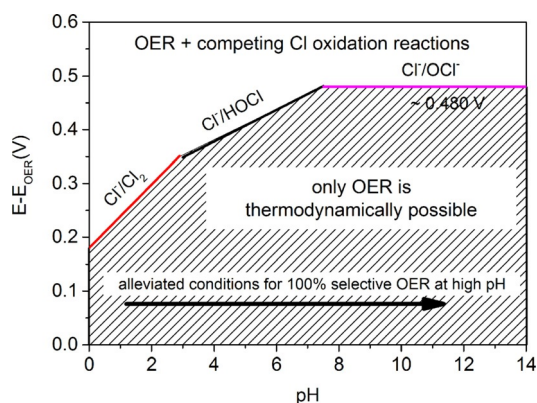
Figure 6. Maximum allowed overpotential of OER electrolyzer catalysts to ensure 100% selective water splitting. Values are obtained as difference between standard electrode potentials of the 3 relevant chloride oxidation reactions (chlorine, hypochlorous acid, and hypochlorite formation) and the OER versus pH. The dahsed area corresponds to oxygen-selective overpotential–pH conditions where thermodynamics point to 100% selective oxygen evolution. Above the limiting lines, chlorine-based reaction products are thermodynamically feasible, yet may be limited by kinetic overpotentials.

potential range (<480 mV, see Figure 6) at technologically targeted current densities of 10 mA cm^{-2}. This is thanks to their very high activity and stability that makes competing chlorine reactions, such as the hypochlorite formation, thermodynamically unfeasible below 1.72 V versus the reversible hydrogen electrode (RHE). Selectivity experiments confirmed the absence of chlorine evolution and a faradaic efficiency of ~100% towards OER under these conditions. Seawater electrolysis with NiFe LDH at neutral pH is limited by the lower activity observed at this pH condition and a strong instability, despite the better stability at near-neutral pH in chloride-free borate buffer. Suppression of chloro-chemistry at technological current densities and near-neutral pH is much more difficult to achieve owing to the lower activity at these pHs. Here, high current densities, and associated low local pH, are a likely resulting from catalyst corrosion. Our data strongly suggest alkaline conditions for seawater oxidation and NiFe LDH as a candidate seawater oxidation catalyst for photoelectrochemical devices and electrolyzers operating at moderate current densities.

Realizing OER-selective seawater electrolysis under acidic conditions where noble metal catalysts, such as Ir or Ru, are required, constitutes a much more severe challenge, as the potential range with high chemical selectivity becomes very narrow (180–350 mV, see Figure 6) within which even the best performing IrO$_x$ catalysts are unable to achieve current densities near or beyond 10 mA cm^{-2}.[27]

In all, we are confident that this first-of-its-kind analysis of the scientific basis of suitable operating conditions of seawater electrocatalysis will aid in the future design of selective seawater electrolyzers and seawater splitting catalysts, which constitutes an important contribution to a future clean power and water supply infrastructure to arid geographical world areas with ocean access.

[1] E. Fabbri, A. Habereder, K. Waltar, R. Kotz, T. J. Schmidt, *Catal. Sci. Technol.* **2014**, *4*, 3800 – 3821.

[2] a) J. E. Bennett, *Int. J. Hydrogen Energy* **1980**, *5*, 401 – 408; b) Y. Surendranath, M. Dinca, D. G. Nocera, *J. Am. Chem. Soc.* **2009**, *131*, 2615 – 2620; c) H. K. Abdel-Aal, K. M. Zohdy, M. Abdel Kareem, *Open Fuel Cells J.* **2010**, *3*, 1 – 7; d) A. A. El-Moneim, N. Kumagai, K. Hashimoto, *Mater. Trans.* **2009**, *50*, 1969 – 1977; e) K. Fujimura, K. Izumiya, A. Kawashima, E. Akiyama, H. Habazaki, N. Kumagai, K. Hashimoto, *J. Appl. Electrochem.* **1999**, *29*, 769 – 775; f) N. Jiang, H. M. Meng, *Surf. Coat. Technol.* **2012**, *206*, 4362 – 4367.

[3] a) W. J. Luo, Z. S. Yang, Z. S. Li, J. Y. Zhang, J. G. Liu, Z. Y. Zhao, Z. Q. Wang, S. C. Yan, T. Yu, Z. G. Zou, *Energy Environ. Sci.* **2011**, *4*, 4046 – 4051; b) K. Maeda, H. Masuda, K. Domen, *Catal. Today* **2009**, *147*, 173 – 178; c) S. M. Ji, H. Jun, J. S. Jang, H. C. Son, P. H. Borse, J. S. Lee, *J. Photochem. Photobiol. A* **2007**, *189*, 141 – 144.

[4] a) H. Y. Su, Y. Gorlin, I. C. Man, F. Calle-Vallejo, J. K. Norskov, T. F. Jaramillo, J. Rossmeisl, *Phys. Chem. Chem. Phys.* **2012**, *14*, 14010 – 14022; b) W. T. Hong, M. Risch, K. A. Stoerzinger, A. Grimaud, J. Suntivich, Y. Shao-Horn, *Energy Environ. Sci.* **2015**, *8*, 1404 – 1427.

[5] S. Trasatti, *Electrochim. Acta* **1984**, *29*, 1503 – 1512.

[6] a) A. R. Zeradjanin, N. Menzel, W. Schuhmann, P. Strasser, *Phys. Chem. Chem. Phys.* **2014**, *16*, 13741 – 13747; b) R. K. B. Karlsson, H. A. Hansen, T. Bligaard, A. Cornell, L. G. M. Pettersson, *Electrochim. Acta* **2014**, *146*, 733 – 740; c) K. S. Exner, J. Anton, T. Jacob, H. Over, *Angew. Chem. Int. Ed.* **2014**, *53*, 11032 – 11035; *Angew. Chem.* **2014**, *126*, 11212 – 11215; d) V. Petrykin, K. Macounova, O. A. Shlyakhtin, P. Krtil, *Angew. Chem. Int. Ed.* **2010**, *49*, 4813 – 4815; *Angew. Chem.* **2010**, *122*, 4923 – 4925; e) K. Macounová, M. Makarova, J. Jirkovsky, J. Franc, P. Krtil, *Electrochim. Acta* **2008**, *53*, 6126 – 6134; f) T. Arikawa, Y. Murakami, Y. Takasu, *J. Appl. Electrochem.* **1998**, *28*, 511 – 516.

[7] WorldChlorineCouncil. Available from http://www.worldchlorine.org/wp-content/themes/brickthemewp/pdfs/sustainablefuture.pdf.

[8] C. Egenhofer, L. Schrefler, V. Rizos, F. Infelise, G. Luchetta, F. Simonelli, W. Stoefs, J. Timini, L. Colantoni, Centre for European Policy Studies, **2014**, p. 25.

[9] EuroChlor, **2012**, p. 48. Available from http://www.eurochlor.org/media/63146/2012-annualreview-final.pdf.

[10] a) M. W. Louie, A. T. Bell, *J. Am. Chem. Soc.* **2013**, *135*, 12329 – 12337; b) C. C. L. McCrory, S. H. Jung, J. C. Peters, T. F. Jaramillo, *J. Am. Chem. Soc.* **2013**, *135*, 16977 – 16987; c) M. Gong, Y. G. Li, H. L. Wang, Y. Y. Liang, J. Z. Wu, J. G. Zhou, J. Wang, T. Regier, F. Wei, H. J. Dai, *J. Am. Chem. Soc.* **2013**, *135*, 8452 – 8455; d) L. Trotochaud, S. L. Young, J. K. Ranney, S. W. Boettcher, *J. Am. Chem. Soc.* **2014**, *136*, 6744 – 6753.

[11] a) C. Du, X. G. Yang, M. T. Mayer, H. Hoyt, J. Xie, G. McMahon, G. Bischoping, D. W. Wang, *Angew. Chem. Int. Ed.* **2013**, *52*, 12692 – 12695; *Angew. Chem.* **2013**, *125*, 12924 – 12927; b) L. Wang, F. Dionigi, N. T. Nguyen, R. Kirchgeorg, M. Gliech, S. Grigorescu, P. Strasser, P. Schmuki, *Chem. Mater.* **2015**, *27*, 2360 – 2366; c) B. Mei, A. A. Permyakova, R. Frydendal, D. Bae, T. Pedersen, P. Malacrida, O. Hansen, I. E. L. Stephens, P. C. K. Vesborg, B. Seger, I. Chorkendorff, *J. Phys. Chem. Lett.* **2014**, *5*, 3456 – 3461.

[12] J. C. Crittenden, R. Rhodes Trussell, D. W. Hand, K. J. Howe, G. Tchobanoglous, *MWH's Water Treatment: Principles and Design, 3rd ed.*, **2012**.

[13] *CRC Handbook of Chemistry and Physics, 96th ed.* (Ed.: D. R. Lide), CRC Press, New York, **2015**.

[14] H. A. Hansen, I. C. Man, F. Studt, F. Abild-Pedersen, T. Bligaard, J. Rossmeisl, *Phys. Chem. Chem. Phys.* **2010**, *12*, 283 – 290.

[15] Y. F. Han, Z. H. Liu, Z. P. Yang, Z. L. Wang, X. H. Tang, T. Wang, L. H. Fan, K. Ooi, *Chem. Mater.* **2008**, *20*, 360 – 363.

[16] D. Friebel, M. W. Louie, M. Bajdich, K. E. Sanwald, Y. Cai, A. M. Wise, M. J. Cheng, D. Sokaras, T. C. Weng, R. Alonso-Mori, R. C. Davis, J. R. Bargar, J. K. Norskov, A. Nilsson, A. T. Bell, *J. Am. Chem. Soc.* **2015**, *137*, 1305 – 1313.

[17] F. Song, X. L. Hu, *Nat. Commun.* **2014**, *5*, 4477.

[18] M. Auinger, I. Katsounaros, J. C. Meier, S. O. Klemm, P. U. Biedermann, A. A. Topalov, M. Rohwerder, K. J. J. Mayrhofer, *Phys. Chem. Chem. Phys.* **2011**, *13*, 16384 – 16394.

[19] a) B. J. Trześniewski, O. Diaz-Morales, D. A. Vermaas, A. Longo, W. Bras, M. T. M. Koper, W. A. Smith, *J. Am. Chem. Soc.* **2015**, *137*, 15112 – 15121; b) M. Dinca, Y. Surendranath, D. G. Nocera, *Proc. Natl. Acad. Sci. USA* **2010**, *107*, 10337 – 10341.

[20] A. M. Smith, L. Trotochaud, M. S. Burke, S. W. Boettcher, *Chem. Commun.* **2015**, *51*, 5261 – 5263.

[21] A. T. Kuhn, C. Y. Chan, *J. Appl. Electrochem.* **1983**, *13*, 189 – 207.

[22] A. J. Bard, L. R. Faulkner, *Electrochemical methods : fundamentals and applications, 2nd ed.*, Wiley, New York, **2001**.

[23] M. J. Kenney, M. Gong, Y. G. Li, J. Z. Wu, J. Feng, M. Lanza, H. J. Dai, *Science* **2013**, *342*, 836 – 840.

[24] R. L. Doyle, I. J. Godwin, M. P. Brandon, M. E. G. Lyons, *Phys. Chem. Chem. Phys.* **2013**, *15*, 13737 – 13783.

[25] M. E. G. Lyons, A. Cakara, P. O'Brien, I. Godwin, R. L. Doyle, *Int. J. Electrochem. Soc.* **2012**, *7*, 11768 – 11795.

[26] W. H. Liu, A. Migdisov, A. Williams-Jones, *Geochim. Cosmochim. Acta* **2012**, *94*, 276 – 290.

[27] a) H. N. Nong, H. S. Oh, T. Reier, E. Willinger, M. G. Willinger, V. Petkov, D. Teschner, P. Strasser, *Angew. Chem. Int. Ed.* **2015**, *54*, 2975 – 2979; *Angew. Chem.* **2015**, *127*, 3018 – 3022; b) H. S. Oh, H. N. Nong, T. Reier, M. Gliech, P. Strasser, *Chem. Sci.* **2015**, *6*, 3321 – 3328; c) T. Reier, M. Oezaslan, P. Strasser, *ACS Catal.* **2012**, *2*, 1765 – 1772; d) T. Reier, D. Teschner, T. Lunkenbein, A. Bergmann, S. Selve, R. Kraehnert, R. Schlögl, P. Strasser, *J. Electrochem. Soc.* **2014**, *161*, F876 – F882.